Biogeosciences Discuss., 9, 4793–4817, 2012
www.biogeosciences-discuss.net/9/4793/2012/
doi:10.5194/bgd-9-4793-2012

Biogeosciences
Discussions

Isotope fractionation between dissolved and suspended particulate Fe in the oxic and anoxic water column of the Baltic Sea

M. Staubwasser[1], R. Schoenberg[2], F. von Blanckenburg[3], S. Krüger[4], and C. Pohl[4]

[1]University of Cologne, Germany
[2]University of Tübingen, Germany
[3]GeoForschungsZentrum Potsdam, Germany
[4]Institute of Baltic Sea Research, Warnemuende, Germany

Received: 14 March 2012 – Accepted: 26 March 2012 – Published: 19 April 2012

Correspondence to: M. Staubwasser (m.staubwasser@uni-koeln.de)

Published by Copernicus Publications on behalf of the European Geosciences Union.

Title Page

Abstract | Introduction

Conclusions | References

Tables | Figures

◀| |▶

◀ ▶

Back | Close

Full Screen / Esc

Printer-friendly Version

Interactive Discussion

Abstract

Fe isotope ratios and concentrations of dissolved Fe (Fe_{dis}, $< 0.45\,\mu m$) and of suspended particulate Fe (Fe_{SPM}) from a depth profile in the Eastern Gotland Basin, Baltic Sea, show a sharp gradient in $\delta^{56}Fe_{dis}$ across the suboxic interface with $\delta^{56}Fe_{dis} = -0.4\,‰$ in the euxinic deep basin and $\delta^{56}Fe_{dis} = +0.3\,‰$ in the oxic upper water column. The isotopic gradient overlaps with a strong concentration gradient of Fe_{dis}, a concentration maximum in Fe_{SPM} and lower $\delta^{56}Fe_{SPM}$ values than $\delta^{56}Fe_{dis}$. These features indicate preferential loss of light Fe isotopes into suspended iron-oxyhydroxides (Fe_{IOH}) during typical oxidative precipitation across the redox interface in the marine environment. The sign of the fractionation, $\Delta^{56}Fe_{Fe\_IOH-Fe(II)(aq)} < 0\,‰$, is in contrast to similar, mostly non-marine redox environments, where $\Delta^{56}Fe_{Fe\_IOH-Fe(II)(aq)} > 0\,‰$. The difference appears to be the result of isotope exchange dominated by reaction kinetics in the marine water column, rather than equilibrium fractionation generally inferred for oxidative Fe precipitation elsewhere. High residual $\delta^{56}Fe_{dis}$ immediately above the suboxic interface and throughout the oxic water column suggest that any potential Fe export from reducing waters or sediments into the open water column is enriched in the heavy isotopes. Within the suboxic to euxinic deep basin the decreasing $\delta^{56}Fe_{SPM}$ trend with depth and a generally low $\delta^{56}Fe_{dis}$ are comparable to trends in marine anoxic sediment profiles indicative of microbial reductive Fe dissolution. This confirms supply of dissolved Fe to the euxinic water column mainly from reductive dissolution of settling particles.

1 Introduction

The fractionation of Fe isotopes between coexisting dissolved and particulate Fe species within the environmental Fe redox cycle often imparts an isotopic signature on residual reaction components (Bullen et al., 2001; Anbar, 2004; Beard and Johnson, 2004). In principle, this may allow the identification of sources of Fe to the modern ocean by using the distinct isotopic signature of diagenetically redox-recycled Fe to discriminate against fluvial, dust and hydrothermal Fe (Severmann et al., 2006; Staubwasser et al., 2006; Anbar and Rouxel, 2007). A recent benthic flux chamber study appears to confirm the efflux of low δ^{56}Fe from early diagenetic recycling (Severmann et al., 2010). With only a few published values for seawater (Lacan et al., 2008; John and Atkins, 2010; Gelting et al., 2010; Radic et al., 2011) and none from anoxic marine basins, however, the database is currently too limited to verify the use of water column Fe isotopes as a direct tracer of diagenetic Fe redox cycling.

Another application of marine Fe isotope fractionation lies in the understanding of the evolution of anoxic oceans and basins of the past by analyzing marine sediments (Jenkyns et al., 2007; Anbar and Rouxel, 2007; Johnson et al., 2008; von Blanckenburg et al., 2008). Of particular interest is the observed occurrence of extremely low δ^{56}Fe in pyrites (δ^{56}Fe between −2 and −4 ‰) prior to the rise of atmospheric oxygen across the Archean-Proterozoic transition approximately 2.3 Ga ago (Rouxel et al., 2005; Johnson et al., 2008). These studies argue for the increasing role of Fe redox cycling at the transition to an oxygenated surface ocean and atmosphere. Authigenic pyrites from sediments of modern anoxic basins, however, only show moderately low δ^{56}Fe values (> −1.5 ‰) (Severman et al., 2008; Fehr et al., 2010). These studies invoke the benthic “iron shuttle” concept of dissolved Fe with diagenetically derived low δ^{56}Fe transported from the shelf to the anoxic deep basin. The applicability of this concept, which was developed in the Black Sea (Wijsman et al., 2001; Anderson and Raiswell, 2004), towards interpreting Proterozoic Fe isotope profiles, however, has not yet been verified directly by water column measurements.

Modern anoxic basins, such as in the Central Baltic Sea, show intense redox cycling of Fe across the redox boundary in the water column by reductive dissolution of Fe_{IOH}, upward diffusion, oxidative precipitation on contact with dissolved oxygen and resettling of particulate Fe_{IOH} (Millero, 2006). Removal from this cycle occurs ultimately by settling of Fe_{IOH} out of the water column and burial. In the euxinic layer below the redox boundary layer, dissolved Fe and dissolved H_2S concentration increases initially with depth to a level where the solubility equilibrium of pyrrhotite (FeS) and greigite (Fe_3S_4) is reached (Landing and Westerlund, 1988; Dyrssen and Kremling, 1990; Lewis and Landing, 1991). Below this depth Fe is ultimately removed from the water column by sulfide precipitation. The high Fe inventory of anoxic basins is thought to be maintained by diagenetic dissolved Fe (Wijsman et al., 2001) or lithogenic reactive Fe (Anderson and Raiswell, 2004) transported from adjacent sediments along the oxic basin's margin.

Fe isotope fractionation may occur along all reactions of the Fe-redox cycle. Reductive microbial dissolution of Fe_{IOH} preferentially releases Fe with a low $^{56}Fe/^{54}Fe$ ratio into solution (Crosby et al., 2007). FeS formation in the euxinic water body preferentially removes light Fe isotopes into the solid phase (Butler et al., 2005). Fe oxidation and precipitation on contact with oxygen in laboratory experiments as well as in continental and estuarine environments leads to a preferential sequestration of heavy isotopes into solid Fe_{IOH} (Bullen et al., 2001; Rouxel et al., 2008). This was found to be consistent with a two-step reaction model of rapid equilibrium isotopic exchange between dissolved redox species and subsequent kinetic fractionation during precipitation (Anbar, 2004; Beard and Johnson, 2004). Accordingly, any dissolved Fe (Fe_{dis}) remaining after Fe_{IOH} precipitation should have a lower $^{56}Fe/^{54}Fe$ ratio than contemporary Fe_{IOH}. Very low $^{56}Fe/^{54}Fe$ ratios should be observable in residual Fe_{dis} after near-quantitative Fe_{IOH} precipitation, which occurs at the redox boundary above anoxic marine basins. Thus, Fe_{dis} exported from marine oxic-anoxic redox boundaries should be isotopically distinguishable. However, this study does not confirm the expectation. The Baltic Sea profile of this study shows high $^{56}Fe/^{54}Fe$ ratios in residual Fe_{dis} above the oxic-anoxic redox boundary and indicates a more prominent role of kinetic isotope fractionation relative to equilibrium exchange in the marine environment.

2 Baltic Sea hydrography and state of Fe redox cycling

The Eastern Gotland Basin (EGB) is the largest of a series of anoxic basins in the Baltic Sea with a maximum depth of 250 m. Anoxic conditions in the Gotland Deep result from an estuarine type circulation pattern in the Baltic Sea, stable stratification (Fig. 1a) and limited exchange of deep water with the adjacent North Sea by a series of shallow sills (Meier et al., 2006). Water column ventilation by winter convection is confined to the upper ∼ 80 m. (Fig. 1b). Deeper water is replaced on average only about once in a decade by storm-induced entrainment of salty water from the North Sea. The last such inflow prior to this study occurred in winter 2003. Monthly monitoring of chemical properties in the EGB show that by the time of this study, in October 2005, anoxic conditions had returned below 125 m depth (Nausch et al., 2008). Euxinic conditions with moderate concentrations of total sulfide (0–60 µM $\sum H_2S$) prevailed below 150 m.

Because the full range of modern marine redox conditions can be observed continuously over the course of many years, the EGB is well suited to study fundamental processes of redox related Fe isotope fractionation in the marine redox Fe cycle. The basin may serve as a close modern analogue to past anoxic oceans. The water column in the EGB displays the typical Fe profile of marine anoxic basins with intense suboxic Fe redox cycling (Fig. 1c). Concentrations of dissolved Fe (Fe_{dis}) of less than 10 nM in the oxic surface layer increase to µM quantities in the euxinic water depending on the season and the number of years since the last inflow event (Pohl et al., 2004; Pohl and Hennings, 2008). The steep concentration gradient sustains upward eddy-diffusion of soluble Fe of up to ∼ 10–15 µmol $m^{-2}\,d^{-1}$ (Pohl and Hennings, 2005). As a consequence of oxidation and precipitation of Fe_{IOH}, a broad maximum of Fe in suspended particulate matter (Fe_{SPM}) occurs across the suboxic to oxic boundary. This Fe_{SPM} maximum overlaps with a general SPM maximum in the turbidity sensor profile (Fig. 1b,c). The ∼ 10 m discrepancy in depth is most likely due to the 2 days difference between Fe sampling and acquisition of the turbidity profile.

A comparison of the fall 2005 profile data of Fe_{dis} and $\sum H_2S$ to the penultimate anoxic period studied in detail during 1981 and 1985 by Dyrssen and Kremling (1990) shows that both Fe_{dis} and $\sum H_2S$ at 180 m are at the low end of concentrations measured in the euxinic waters. The 2005 data are well below the equilibrium concentrations of FeS indicative of sulfide precipitation and determined for the euxinic profiles in 1981 and 1985. FeS precipitation below the sampled depth in 2005, however, may have occurred.

3 Water column sampling and analytical methods

3.1 Water column sampling by pump-CTD and in-line filtration

The site of sampling was monitoring station 271 at 57° 18,3′ N and 20° 4,6′ E in the Eastern Gotland Basin. All water samples were pumped by a trace metal suitable pump-CTD (P-CTD) system (Strady et al., 2008) fitted with a metal-free carbon fiber pump. The P-CTD allows CTD and O_2 profiling, continuous water sampling from up to 400 m depth and subsequent in-line filtration (see below) without exposure to atmosphere. To avoid memory effects from particles desorbing from the pump tube walls, the system was allowed 15 min of flushing time prior to sampling. To check against potential memory effects introduced by pumping particle-loaded seawater through more than 200 m of tubing, concentration measurements were also performed on a parallel bottle cast. Measured values were within agreeable limits with one notable exception from 100 m depth. This particular sample showed enrichment in soluble Fe concentration by a factor of two for the P-CTD and corresponding factor-two depletion in suspended Fe. This most likely indicates disintegration of particles during the pumping process. Accordingly, this sample was discarded from the list of isotope data (Table 1). Other non-trivial variability between bottle-casts and P-CTD measurements (e.g. 150 m) was only observed within either the soluble or suspended fraction, respectively. These differences compare well with natural variability between parallel bottle-cast profiles from previous studies. Such variability is most likely the result of water column inhomogeneity and internal waves which are readily observable during dissolved oxygen and turbidity monitoring over the course of a few hours. All data are summarized in Table 1.

Samples for trace metal concentration and for Fe isotope analysis were taken from parallel profiles. Samples for concentration measurements were processed according to established monitoring procedures (Pohl et al., 2004). For Fe isotope analysis, two liters were filtered in-line directly from the P-CTD through acid-clean 0.45 µ PTFE filters (Millipore hydrophilic PTFE) in a PFA housing (Savillex). High particle loads required one change of filter for each liter of seawater filtered. Samples were acidified with double distilled HNO_3 to pH ≈ 2 and stored until processing and analysis on shore. All handling of samples and filters on board was performed inside an ISO 5 (class-100) laminar flow hood.

3.2 Concentration and isotope analysis

Samples for Fe concentration were analyzed by AAS after pre-concentration (Pohl et al., 2004). For the isotope analysis of soluble Fe, a ^{54}Fe-^{58}Fe double spike approach was used. The spike was calibrated against IRMM-14 standard and an in-house Fe solution (JM puratronic, δ^{56}FeIRMM = 0.42). The δ^{56}FeIRMM values (in short, δ^{56}Fe) are defined as:

$$\delta^{56}\mathrm{Fe} = \frac{(^{54}\mathrm{Fe}/^{56}\mathrm{Fe})_{\mathrm{sample}}}{(^{54}\mathrm{Fe}/^{56}\mathrm{Fe})_{\mathrm{IRMM\text{-}14}}} - 1 \qquad (1)$$

The double spike was added to sample aliquots ranging from 20–1000 ml (according to Fe concentration) and allowed 24 h of equilibration time. An experimental study on Fe isotope equilibrium exchange between inorganic and siderophore-complexed Fe (Dideriksen et al., 2008) confirms complete spike-sample equilibration within this time. Fe was co-precipitated with $Mg(OH)_2$ twice by addition of ammonia (Wu, 2007). The precipitation may not be entirely quantitative at the presence of strong Fe-binding organic ligands (Dideriksen et al., 2008), but the double spike calculation procedure corrects internally for any potential mass-dependent fractionation due to loss during separation chemistry as well as instrumental fractionation due to any potential residual matrix present in the analysis solution and the substantial mass bias introduced by the mass spectrometer's interface (Schoenberg et al., 2008). After ion exchange separation (Schoenberg and von Blanckenburg, 2005), measurements were made on 200–400 ng Fe with a ThermoFinnigan Neptune MC-ICP-MS and an ESI Apex-Q desolvator. Mass bias was corrected internally and monitored by bracketing standards. Possible interference by ^{54}Cr and ^{58}Ni were monitored through ^{52}Cr and ^{60}Ni. Combinations or H, C, N and O from residual organic components and of the same elements with Ar that may add up to interfere with the four Fe isotopes are resolved by measuring in the instrument's medium resolution mode, which has a mass resolution of $m/\Delta m \approx 8000$ (10 % valley).

Particulate Fe was leached from the PTFE filters with aqua regia at 120 °C, purified by ion-exchange and measured by standard bracketing. Internal analytical uncertainty (2 sigma) was 0.1 ‰ (δ^{56}Fe) for both methods. Total blanks were measured by isotope dilution and did not exceed 20 ng for the separation procedure from seawater and 15 ng for the filter samples.

4 Results and discussion

Both the dissolved and suspended matter profiles show systematic isotope trends with depth (Fig. 1d). The $\delta^{56}\mathrm{Fe}_{\mathrm{dis}}$ in the oxic layer is persistently higher than in the anoxic layer with a sharp transition at the redox transition. The profile of $\delta^{56}\mathrm{Fe}_{\mathrm{SPM}}$ shows the lowest values in the depth interval from the suboxic layer to the top of the halocline at ~ 70 m, but includes some scatter at 130 and 100 m, i.e. within and immediately above the suboxic layer. In the following, the profiles will be discussed in terms of chemical reactions and transport paths along the typical internal marine Fe redox cycle of anoxic basins (Millero, 2006) in turn for the suboxic layer, the (mildly) euxinic layer at greater depth, and the oxic surface layer.

4.1 Fe isotope fractionation across the suboxic layer

4.1.1 The relationship between $\delta^{56}Fe_{dis}$ and $\delta^{56}Fe_{SPM}$

Below the suboxic layer at depths greater than 150 m $\delta^{56}Fe_{dis}$ is fairly constant at ~ -0.4 ‰. Between 150 m and 115 m depth, across the suboxic zone and the oxic boundary, values of $\delta^{56}Fe_{dis}$ increase from −0.4 ‰ to +0.3 ‰ along with a corresponding decrease of dissolved Fe concentration and a maximum in both turbidity and suspended Fe (Fig. 1b–d). The $\delta^{56}Fe_{SPM}$ values change from being higher than corresponding $\delta^{56}Fe_{dis}$ below the base of the suboxic layer at 150 m depth, with $\delta^{56}Fe_{SPM} = 0.1$ ‰, to lower than $\delta^{56}Fe_{dis}$ inside the suboxic layer, where $\delta^{56}Fe_{SPM}$ values reach ±0.4 ‰. Concentration profiles in the EGB during this and previous cruises (Pohl et al., 2004; Pohl and Hennings, 2005, 2008) are similar to anoxic basin profiles in general (Millero, 2006) and are typically viewed as the result of upwards diffusion, oxidation of Fe_{dis}, removal by precipitation and subsequent settling across the suboxic layer.

Precipitation most likely results in the formation of Fe_{IOH} particles in the colloidal size spectrum initially, but the maximum in Fe_{SPM} concentration within the suboxic layer indicates rapid coagulation and ultimate removal from Fe_{dis}. The corresponding isotopic trend upwards along the profile suggests that the loss of Fe_{dis} due to oxidation-precipitation is accompanied by preferential loss of light Fe isotopes. This causes $\delta^{56}Fe_{SPM}$ to become lower than the corresponding residual $\delta^{56}Fe_{dis}$. Ideally, in a closed system with in situ Fe_{IOH} precipitation after oxidation, mass-balance requires that the trend in $\delta^{56}Fe_{SPM}$ should follow $\delta^{56}Fe_{dis}$ with a corresponding negative offset. This may indeed be the case for the two upper samples near the oxic-suboxic boundary, but sample resolution is too low for a definite conclusion. In the EGB suboxic layer, some preformed particles, such as detrital reactive Fe_{IOH} and Fe-bearing silicates, either settling from above or transported laterally, most likely contribute to the total pool of Fe_{SPM} and obscure the expected trend. In addition, the redox boundary shoals and deepens by about 10 m seasonally (Pohl et al., 2004), so that different generations of precipitated particles from different horizons in the redox sequence may mix to some degree with actually precipitated particles. A minor role of silicates can be inferred for the turbidity maximum by using trace element data of a previous study conducted in 2000 (Pohl et al., 2004). The Fe_{SPM} fraction per total particle mass showed a fourfold increase in the suboxic layer that was not matched by other trace elements generally associated with silicates, such as Ni. Accordingly, non-silicate material, such as Fe_{IOH} must dominate the particle maximum. This suggests that the Fe rich particle maximum is mostly the consequence of diffusion controlled oxidation and precipitation in situ rather than Fe_{IOH} resuspended from silicate-rich sediments from the basin's margin. In addition, there is no apparent density boundary (Fig. 1a) that would support a vertically tightly confined layer of resuspended material. Because the depth of the Fe_{SPM} maximum shows the same seasonal shallowing as the redox boundaries (Pohl et al., 2004), redox cycling of Fe is the most plausible explanation for its presence.

4.1.2 Kinetic control of isotope fractionation during Fe oxidation and precipitation in the suboxic Eastern Gotland Basin

Light Fe isotope removal across the redox boundary in the EGB on oxidative precipitation is the opposite compared to previous experimental and observational Fe isotope data from a variety of similar redox environments, including continental streams, anoxic lakes, estuarine groundwater discharge plumes, and controlled microbial experiments, but not marine anoxic basins (Bullen et al., 2001; Anbar, 2004; Beard and Johnson, 2004; Rouxel et al., 2008). The observed Fe isotope fractionation in these studies matches controlled Fe oxidation and precipitation experiments with high micromolar concentrations of Fe and $pH < 7$ (Bullen et al., 2001; Skulan et al., 2002; Welch et al., 2003; Beard and Johnson, 2004; Croal et al., 2004; Busigny et al., 2008; Teutsch et al., 2009). The isotope reaction is commonly explained with a simplified two-step reaction model, $\text{Fe(II)}_{\text{aq}} \leftrightarrow \text{Fe(III)}_{\text{aq}} \rightarrow \text{Fe}_{\text{IOH}}$ and an overall effective fractionation factor, $\Delta^{56}\text{Fe}_{\text{FOH-Fe(II)}}$ (Anbar, 2004; Beard and Johnson, 2004). Under the prevailing conditions in the above studies, isotopic equilibrium is achieved rapidly between dissolved redox species with a ~ 3 ‰ enrichment of the heavier isotope in the $\delta^{56}\text{Fe}$ of Fe(III) (Welch et al., 2003), followed by a kinetic 1–2 ‰ depletion of Fe_{IOH} in the heavier isotope on precipitation (Skulan et al., 2002). The combination of both sets the effective overall fractionation factor $\Delta^{56}\text{Fe}_{\text{FOH-Fe(II)}} > 0$ ‰ or $\alpha^{56}\text{Fe}_{\text{FOH-Fe(II)}} > 1$, respectively (Anbar, 2004; Beard and Johnson, 2004). Observations quoted above, all with micromolar Fe concentration and pH at or lower than neutral, fit that reaction model. However, in the EGB, the effective $\Delta^{56}\text{Fe}_{\text{FOH-Fe(II)aq}} < 0$ ‰, rather than > 0 ‰, or effective $\alpha^{56}\text{Fe}_{\text{FOH-Fe(II)aq}} < 1$ rather than > 1, respectively.

Theoretical studies (Anbar, 2004; Beard and Johnson, 2004) highlight the dependence of effective $\Delta^{56}\text{Fe}_{\text{FOH-Fe(II)aq}}$ on the relative magnitude of reaction rate constants of the two sequential reaction steps, $\text{Fe}^{2+}\text{(aq)} \leftrightarrow \text{Fe}^{3+}\text{(aq)} \rightarrow \text{Fe}_{\text{IOH}}$, where k_1 describes the (pseudo-first order) removal rate of Fe^{2+}(aq) by oxidation, the back reduction rate is k_{-1}, and k_2 is the removal rate of Fe^{3+}(aq) by Fe_{IOH} precipitation. The effective $\Delta^{56}\text{Fe}_{\text{FOH-Fe(II)aq}} = 0.9$ ‰ observed in laboratory experiments (Bullen et al., 2001) was reproduced in a model calculation (henceforth BJ04) for a ratio of reaction rates $k_2/k_1 = 5$ (Beard and Johnson, 2004). Fractionation factors for the individual steps were $\Delta^{56}\text{Fe}_{\text{Fe(III)aq-Fe(II)aq}} = 2.9$ ‰ equilibrium redox reaction, and $\Delta^{56}\text{Fe}_{\text{FOH-Fe(III)aq}} = -2.0$ ‰ for the kinetic precipitation reaction. Rapid isotopic equilibration was invoked (Anbar, 2004; Beard and Johnson, 2004), which requires rapid back-reduction, i.e. a large k_{-1}. Using the BJ04 model, with the same fractionation factors and the same ratio of k_2/k_1, the expected composition of residual Fe_{dis} above the suboxic layer of the EGB would be $\delta^{56}\text{Fe} = -2.7$ ‰ at ~ 95 % Fe_{dis} removal from an initial $\delta^{56}\text{Fe}_{\text{dis}} = -0.4$ ‰ at the top of the EGB euxinic layer. This value is very different from the measured value above the EGB oxic-suboxic interface ($\delta^{56}\text{Fe}_{\text{dis}} = +0.3$ ‰). Thus, the reaction scheme of $\text{Fe(II)}_{\text{aq}} \leftrightarrow \text{Fe(III)}_{\text{aq}} \rightarrow \text{Fe}_{\text{IOH}}$

Title Page
Abstract | Introduction
Conclusions | References
Tables | Figures
◀| |▶
◀ ▶
Back | Close
Full Screen / Esc
Printer-friendly Version
Interactive Discussion

with rapid isotopic equilibrium reached in the first reaction step, feasible for the previous studies quoted above, cannot explain observations in the EGB. This suggests that isotopic equilibrium is not reached during the redox reaction step.

The magnitude of reaction rates k_1 and k_2 during Fe_{dis} oxidation-precipitation, and consequently the effective isotope fractionation factor $\Delta^{56}Fe_{FOH\text{-}Fe(II)aq}$, depends on the concentration of Fe_{dis} but also on the types of inorganic ligands present (such as rapidly oxidizing Fe-hydroxide and Fe-carbonate species, which are themselves a function of pH and dissolved inorganic carbon); the presence of organic ligands; and possibly the presence of colloidal forms of Fe (King 1998; Rose and Waite, 2002; Santana-Casiano et al., 2005; Pham and Waite, 2008). Although the various components may result in complex reaction paths that cannot be unraveled without an experimental setup well beyond the scope of this study, the two-step model may be used to discriminate between kinetic and equilibrium domination of the effective fractionation factor of the total reaction. At favorable ambient environmental conditions, when precipitation ($Fe^{3+} \rightarrow Fe_{IOH}$) out-competes the back reduction of the preceding equilibration reaction ($Fe^{2+} \leftrightarrow Fe^{3+}$), kinetic rather than equilibrium isotope exchange dominates the redox exchange reaction (Anbar, 2004). The observed trend in the EGB towards $\delta^{56}Fe_{dis} = +0.3‰$ may be achieved using BJ04 with a ratio of $k_2/k_1 \sim 0.7$, which is equal to a much higher forward rate (k_1) than in the original model or a lower backward reaction rate (k_{-1}), respectively.

The EGB differs from previously studied environments as the Fe concentration is only nanomolar (Fig. 1c). In addition, the pH > 7 and alkalinity is high, as indicated by measurements of the monthly Swedish monitoring program made a few weeks before this cruise (Fig. 2). Controlled oxidation-precipitation experiments in artificial seawater at ~ 100 nM Fe_{dis} concentration (Pham and Waite, 2008) – similar to the observed concentration in the EGB suboxic layer (~ 30–100 nM) – indeed suggest a strong increase of k_1 over k_{-1} at marine pH conditions similar to the EGB. The back-reduction of dissolved Fe^{3+} is also inhibited at the presence of suspended Fe_{IOH} and isotopic equilibrium may therefore not be reached in the EGB suboxic layer. As the back reaction (reduction) becomes less efficient, the redox reaction becomes increasingly kinetic.

4.1.3 Reaction paths

The experiments by Pham and Waite (2008) highlight an inorganic reaction path for Fe oxidation and precipitation. The Fe isotopic exchange between inorganic species under alkaline pH, high alkalinity, and high $\mathrm{Fe_{SPM}}$ conditions prevailing in the EGB (Figs. 1c and 2) would be kinetically controlled by an enhanced oxidation rate (k_1) due to rapidly oxidized Fe-carbonate species and a low back reduction rate (k_{-1}) due to competition with rapid precipitation at alkaline pH. A similar kinetic fractionation dominance my in principle be achieved with a purely organic-ligand controlled reaction path, but is more difficult to align with dissolved Fe(II) species measurements in the Baltic Sea (Breitbarth et al., 2009) and the comparable Black Sea environment data (Lewis and Landing, 1991; Yemenicioglu et al., 2006). The presence of free $\mathrm{Fe^{2+}}$(aq) and a considerable fraction of inorganic colloidal Fe rules out quantitative oxidation followed by sluggish precipitation from an organic ligand-bound pool of dissolved Fe(III), which could be an alternative explanation considering Fe-isotope fractionation factors alone (Dideriksen et al., 2008). However, even if organic ligands are significantly involved in the overall reaction, an overall kinetic dominance of the isotope reaction remains currently the most plausible conclusion. It is noteworthy, that the observation of initially light $\mathrm{Fe_{SPM}}$ gaining isotopically heavy Fe from $\mathrm{Fe_{dis}}$ in the EGB is identical to a recent observation in a buoyant hydrothermal plume of a basaltic vent system in the Atlantic (Bennet et al., 2009), an environment of generally similar redox chemistry, pH and alkalinity, comparable concentration of dissolved and particulate Fe, and low content of organic ligands.

In absence of experimentally defined Fe isotope fractionation factors, or even detailed analysis of the Fe-species present in the EGB suboxic water during this study, other individual effects due to Fe-speciation are difficult to discuss even in qualitative terms. However, a number of possible alternative reaction paths appear unlikely with respect to the canonical two-step reaction scheme $Fe(II)_{aq} \leftrightarrow Fe(III)_{aq} \rightarrow Fe_{IOH}$ considering the currently available data. For instance, adsorption of Fe^{2+} onto preformed Fe_{IOH} surfaces favors removal of heavy Fe isotopes from solution (Crosby et al., 2007; Mikutta et al., 2009) and cannot explain the observed $\Delta^{56}Fe_{FOH\text{-}Fe(II)aq} < 0$. Another process, the coagulation of colloids and subsequent settling is likely to occur in principle, but unlikely to affect the measured overall fractionation between dissolved Fe ($< 0.45\,\mu m$) and suspended matter $> 0.45\,\mu m$ in a fundamental way because such coagulation itself does not lead to significant Fe isotope fractionation (Bennett et al., 2009; Escoube et al., 2009). The overall effect observable in the concentration profile is a transfer of isotopically light Fe_{dis} into Fe_{SPM} (Fig. 1d). The sign change of the overall fractionation factor in comparison to the other environmental studies so far in particular is unlikely to be the result of colloid coagulation.

4.2 Fe isotopes in the euxinic zone

Discussion of the euxinic water column is limited to its upper, only mildly euxinic part (150–180 m depth). Here, the Fe_{dis} concentration profile in the light of previously defined conditions of FeS precipitation in the EGB (Dyrssen and Kremling, 1990) indicates that conditions of sulfide precipitation had not yet been reached at that depth in the most recent stagnant period of the EGB at the time of sampling. Sulfide precipitation would also contrast with minimal Fe_{SPM} concentration and increasingly higher $\delta^{56}Fe_{SPM}$ values than $\delta^{56}Fe_{dis}$, the opposite fractionation than expected for sulfide precipitation (Butler et al., 2005). Sulfides present at the surface sediments in the Gotland basin also have a much lower $\delta^{56}Fe$ (around −1.5 ‰, Fehr et al., 2010). In the following, two variants of microbial iron reduction as an alternative reaction path and their likely Fe isotopic evolution will be discussed in order to explain the observations.

In the sampled euxinic part of the EGB, negative $\delta^{56}Fe$ values of Fe_{dis} prevail ($\delta^{56}Fe_{dis} \sim -0.4$ ‰, Fig. 1c). HCl-leachable Fe in EGB sediments, a crude approximation of reactive Fe (Poulton and Canfield, 2005), ranges from $\delta^{56}Fe = -0.27$ to $+0.21$

(Fehr et al., 2010). Euxinic EGB $\delta^{56}Fe_{dis}$ values of ~ -0.4 ‰ could therefore in principle be the result of early diagenetic dissimilatory reduction of Fe_{IOH} in the sediments and subsequent efflux of low $\delta^{56}Fe_{dis}$ into the water column. However, the generally higher sulfide concentration in interstitial water than in the overlying water column and common amorphous FeS precipitation in the EGB sediments (Carman and Rahm, 1997; Fehr et al., 2010) limits such efflux from the euxinic sediments. An alternative explanation for the EGB euxinic $\delta^{56}Fe_{dis}$ values is dissimilatory Fe reduction in the water column, which is an established reaction in such environments (Anderson and Raiswell, 2004). The observed increase in EGB $\delta^{56}Fe_{SPM}$ from −0.4 to −0.1 ‰ between euxinic depths of 150 and 170 m is similar to typical early-diagenetic sedimentary reactive Fe profiles where iron reducing microbes mobilize Fe and leave the residual Fe_{IOH} enriched in heavy Fe isotopes (Staubwasser et al., 2006). A minimum in Fe_{SPM} concentrations and a $\delta^{56}Fe_{dis}$ in the mildly euxinic EGB water column sampled here are similar to $\delta^{56}Fe_{SPM}$ in the overlying suboxic layer. This suggests a simple near-quantitative mass transfer of reactive Fe_{IOH} into dissolved Fe (< 0.45 µm). Microbial reductive dissolution of a fraction of sinking Fe_{IOH} particles in the water column is therefore a likely alternative explanation for increasing concentrations of Fe_{dis}. The direct transformation of Fe_{IOH} to Fe sulfides, as suggested by Dyrssen and Kremling (1990) and demonstrable by low fractions of soluble Fe^{2+} within total euxinic Fe_{dis} (Breitbarth et al., 2009), is compatible with the above interpretation. Such transformation between solid phases appears to take place without Fe isotope fractionation, at least in the sediment column (Staubwasser et al., 2006) and therefore would not affect Fe isotope ratios in Fe_{SPM}. As suggested for sedimentary early diagenesis, the decreasing concentration of Fe_{IOH} is probably due to competing dissimilatory Fe reduction (producing truly soluble Fe^{2+} and isotopically altered Fe_{SPM}) as well as Fe_{SPM} disintegration and transformation to FeS (producing dissolved Fe(II) < 0.45 µm of the same isotopic composition as initial Fe_{SPM}). Thus, the EGB data lend support to the conclusion by Anderson and

Raiswell (2004) that the high inventory of Fe_{dis} in marine anoxic basins is maintained by dissolution of reactive Fe_{IOH} particles.

4.3 Fe isotopes in oxic water layer

Fe isotope fractionation in the surface layer cannot be discussed in a representative fashion for the lack of sampling detail. The uppermost two samples of δ^{56} Fe_{SPM} (−0.1 to −0.2 ‰) in this study from the EGB compare well with the range of −0.05 to −0.3 ‰ measured in near surface particulate Fe above Landsort Deep (Gelting et al., 2010), another basin in the Central Baltic proper. The oxygen-rich lower water column of the EGB shows high $\delta^{56}Fe_{dis}$ similar to values in the surface mixed layer. These are not explainable with low $\delta^{56}Fe_{dis}$ efflux described from suboxic sediments present along the basins margin as observed in a similar environment elsewhere (Severmann et al., 2010) and inferred from surface sediment measurements from the EGB (Fehr et al., 2010). This may suggest that any low δ^{56}Fe efflux is rapidly transferred into a particulate phase by oxidative precipitation with the kinetic fractionation described above. Alternative explanations, which remain to be verified by pore water measurements, are that the efflux from suboxic EGB sediments is not significant, or the efflux does not have a low δ^{56}Fe. The isotopic composition in the upper water column of the EGB may readily be explained by deep overturning in winter and mixing of high $\delta^{56}Fe_{dis}$ from soluble Fe just above the suboxic zone, but see Breitbarth et al. (2009) for a different conclusion. An influence by local runoff from land cannot currently be addressed from an isotopic perspective for lack of data.

5 Conclusions

Kinetic isotope fractionation dominates the marine water column Fe redox cycle in the EGB. Consequently, fractionation factors will change with reaction rates. The controls on reaction rates themselves have been described in detail in previous studies (King, 1998; Rose and Waite, 2002; Santana-Casiano et al., 2006; Pham and Waite, 2008) and include the concentration of dissolved Fe, the concentration of suspended particulate Fe_{IOH}, and the abundance of fast reacting Fe species. The inorganic rapidly oxidizing species in the marine environment are Fe complexes with OH^- and CO_3^{2-}, whose presence is favored in the marine environment at pH above neutral and high alkalinity.

The water column data presented here suggest, that if the "benthic Fe shuttle" is active in the Eastern Gotland Basin (EGB), transport from the oxic shelf to the euxinic deep EGB is likely dominated by lithogenic reactive Fe from the oxic margins as suggested by Anderson and Raiswell (2004). There is no low δ^{56}Fe efflux from redox processes within the EGB detectable in the isotope data of the water column. In fact, $\delta^{56}Fe_{dis}$ immediately above the redox boundary is the isotopically heaviest Fe in the basin. From anoxic basins like the EGB, low δ^{56}Fe from diagenetic redox cycling may be exported as a precipitate of suspended particulate reactive Fe above the redox interface. If the possibly pH dependent dominance of kinetic fractionation during oxidative Fe precipitation can be confirmed to be true in general, then low δ^{56}Fe diagentic efflux observed in benthic chamber studies (Severmann et al., 2010) can only be transferred into the generally alkaline open ocean water column in dissolved form if stabilized in solution without the occurrence of oxidative precipitation. If oxidative precipitation occurs, low $\delta^{56}Fe_{dis}$ diagenetic efflux may be traceable in the water column through the $\delta^{56}Fe_{SPM}$ fraction.

Outgoing fluxes of Fe from the EGB anoxic water column, i.e. residual Fe_{dis} above the redox-cline and Fe_{SPM} eventually settling onto the seafloor, are both enriched in heavy Fe isotopes relative to ingoing fluxes of Fe_{SPM}, assuming that suspended matter is equal to the settling material. Consequently, Fe redox cycling in the EGB retains light isotopes within the anoxic water column by internal recycling. In general, intense redox recycling may therefore draw an anoxic basin's overall isotopic composition towards low δ^{56}Fe values. Ranging from $\delta^{56}\mathrm{Fe} = -0.6$ to $+0.4$ ‰, the Gotland Basin profile on average is only slightly below average crustal value $\delta^{56}\mathrm{Fe} \sim 0$ ‰ (Beard et al., 2003).

This suggests that the basin's Fe isotopic inventory is largely dominated by reactive Fe supply from adjacent lands, which nevertheless is intensely recycled across the basin's redox boundaries. In general, the Fe isotope composition of an anoxic basin's water column and of its authigenic minerals should reflect the proportion of Fe recycled within the basin versus Fe supplied from external sources. A large inventory of Fe combined with intense redox recycling and relatively low detrital Fe_{IOH} input may principally lead to very low δ^{56}Fe values of the basin's reactive Fe inventory. Such a scenario would be conceivable on a larger scale during times of low atmospheric oxygen and high seawater concentration of dissolved Fe in the early and mid-Proterozoic and may provide an explanation for the very low δ^{56}Fe values found in pyritic shale deposited prior to 2.3 Ga yr ago.

Acknowledgements. The authors thank the masters and crews of the FS Alkor and FS Professor A. Penck for their professional assistance during the two cruises that contributed to the presented results. This study was supported by a DFG grant to MS and FvB.

References

Anbar, A. D.: Iron stable isotopes: beyond biosignatures, Earth Plan. Sci. Lett., 217, 223–236, 2004.

Anbar, A. D. and Rouxel, O.: Metal stable isotopes in paleoceanography, Annu. Rev. Earth Pl. Sc., 3, 717–746, 2007.

Anderson, T. F. and Raiswell, R.: Sources and mechanisms for the enrichment of highly reactive Fe in euxinic sediments of the Black Sea sediments, Am. J. Science, 304, 203–233, 2004.

Bennett, S. A., Rouxel, O., Schmidt, K., Garbe-Schönberg, D., Statham, P. J., and German, C. R.: Iron Isotope fractionation in a buoyant hydrothermal plume, 5° S Mid-Atlantic Ridge, Geochim. Cosmochim. Acta, 73, 5619–5634, 2009.

Beard, B. L. and Johnson, C. M.: Fe isotope variations in the modern and ancient earth and other planetary bodies, Rev. Min. Geochem., 55, 319–357, 2004.

Beard, B. L., Johnson, C. M., Skulan, J. L., Nealson, K. H., Cox, L., and Sun, H.: Application of Fe isotopes to tracing the geochemical and biological cycling of Fe, Chem. Geol., 195, 87–117, 2003.

von Blanckenburg, F., Marnberti, M., Schoenberg, R., Kamber, B., and Webb, G. E.: The iron isotope composition of microbial carbonate, Chem. Geol., 249, 113–128, 2008.

Breitbarth, E., Gelting, J., Walve, J., Hoffmann, L. J., Turner, D. R., Hassellóv, M., and Ingri, J.: Dissolved iron (II) in the Baltic Sea surface water and implications for cyanobacterial bloom development, Biogeosciences, 6, 2397–2420, doi:10.5194/bg-6-2397-2009, 2009.

Bullen, T. D., White, A. F., Childs, C. W., Vivit, D. V., and Schulz, M. S.: Demonstration of significant abiotic iron isotope fractionation in nature, Geology, 29, 699–702, 2001.

Busigny, V., Jezequel, D., Louvat, P., Viollier, E., and Michard, G.: Iron isotopes in Lake Pavin (French Massif Central): a window to the Precambrian ocean, Eos Trans. AGU, 89(53), Fall Meet. Suppl., PP31C-1510, 2008.

Butler, I. B., Archer, C., Vance, D., Oldroyd, A., and Rickard, D.: Fe isotope fractionation on FeS formation in ambient aqueous solution, Earth Plan. Sci. Lett., 236, 430–442, 2005.

Carman, R. and Rahm, L.: Early diagenesis and chemical characteristics of interstitial water and sediments in the deep deposition bottoms of the Baltic proper, J. Sea Res., 37, 25–47, 1997.

Croal, L. R., Johnson, C. M., Beard, B. L., and Newman, D. K.: Iron isotope fractionation by Fe(II)-oxidizing photoautotrophic bacteria, Geochim. Cosmochim. Acta, 68, 1227–1242, 2004.

Crosby, H. A., Roden, E. E., Johnson, C. M., and Beard, B. L.: The mechanisms of iron isotope fractionation produced during dissimilatory Fe(III) reduction by Shewanella putrefaciens and Geobacter sulfurreducens, Geobiology, 5, 169–189, 2007.

Dideriksen, K., Baker, S. A., and Stipp, S. L. S.: Equilibrium Fe isotope fractionation between inorganic aqueous Fe(III) and the siderophore complex, Fe(III)-desferrioxamine B, Earth Plan. Sci. Lett., 269, 280–290, 2008.

Dyrssen, D. and Kremling, K.: Increasing hydrogen sulfide concentration and trace metal behavior in the anoxic Baltic waters, Mar. Chem., 30, 193–204, 1990.

Escoube, R., Rouxel, O. J., Sholkovitz, E., and Donard, O. F. X.: Iron isotope systematics in estuaries: the case of North River, Massachusetts (USA), Geochim. Cosmochim. Acta, 73, 4045–4059, 2009.

Fehr, M. A., Andersson, P. S., Halenius, U., Gustafsson, Ö., and Mörth, C. M.: Iron enrichments and Fe isotopic compositions of surface sediments from the Gotland Deep, Baltic Sea, Chem. Geol., 227, 310–322, 2010.

Gelting, J., Breitbarth, E., Stolpe, B., Hassellöv, M., and Ingri, J.: Fractionation of iron species and iron isotopes in the Baltic Sea euphotic zone, Biogeosciences, 7, 2489–2508, doi:10.5194/bg-7-2489-2010, 2010.

Grasshoff, K., Ehrhardt, M., Kremling, K., and Anderson, L. G.: Methods of Seawater Analysis, Wiley-VCH, Hoboken, 1983.

Jenkyns, H. C., Matthews, A., Tsikos, H., and Erel, Y.: Nitrate reduction, sulfate reduction, and sedimentary iron isotope evolution during the Cenomanian-Turonian oceanic anoxic event, Paleoceanography, 22, PA3208, doi:10.1029/2006PA001355, 2007.

John, S. G. and Atkins, J. F.: Analysis of dissolved iron isotopes in seawater, Mar. Chem., 119, 65–76, 2010.

Johnson, C. M., Beard, B. L., and Roden, E. E.: The iron isotope fingerprints of redox and biogeochemical cycling in the modern and ancient earth, Annu. Rev. Earth Pl. Sc., 36, 457–493, 2008.

Karlson, B., Axe, P., Funkquist, L., Kaitala, S., and Sørensen, K.: Infrastructure for marine monitoring and operational oceanography, in: Reports Oceanography, 39, Swedish Meteorological and Hydrological Institute, Norrköping, 101 pp., 2009.

King, D. W.: Role of carbonate speciation on the oxidation rate of Fe(II) in aquatic systems, Environ. Sci. Tech., 32, 2997–3003, 1998.

Lacan, F., Radic, A., Jeandel, C., Poitrasson, F., Sarthou, G., Pradoux, C., and Freydier, R.: Measurement of the isotopic composition of dissolved iron in the open ocean, Geophys. Res. Lett., 35, GL24610, doi:10.1029/2008GL035841, 2008.

Landing, W. M. and Westerlund, S.: The solution chemistry of iron(II) in Framvaren Fjord, Mar. Chem., 23, 329–343, 1988.

Lewis, B. L. and Landing, W. M.: The biogeochemistry of manganese and iron in the Black Sea, Deep-sea Res., 38, 773–803, 1991.

Meier, H. E. M., Feistel, R., Piechura, J., Arneborg, L., Burchard, H., Fiekas, V., Golenko, N., Kuzmina, N., Mohrholz, V., Nohr, C., Paka, V. T., Sellschopp, J., Stips, A., and Zhurbas, V.: Ventilation of the Baltic Sea deep water: a brief review of present knowledge from observation and models, Oceanologia, 48(S), 133–164, 2006.

Mikutta, C., Wiederhold, J. G., Cirpka, O. A., Hofstetter, T. B., Bourdon, B., and von Gunten, U.: Iron isotope fractionation and atom exchange during sorption of ferrous iron to mineral surfaces, Geochim. Cosmochim. Acta, 73, 1795–1812, 2009.

Millero, F. J.: Chemical Oceanography, CRC Press, Boca Raton, 2006.

Nausch, G., Nehring, D., and Nagel, K.: Nutrient concentration, trends and their relation to eutrophication, in: State and Evolution of the Baltic Sea, 1952–2005, Feistel, R., Nausch, G., and Wasmund, N. (eds.), Wiley, Hoboken, 337–366, 2008.

Pham, A. N. and Waite, T. D.: Oxygenation of Fe(II) in natural waters revisited: kinetic modeling approaches, rate constant estimation and the importance of various reaction pathways, Geochim. Cosmochim. Acta, 72, 3616–3630, 2008.

Pohl, C. and Hennings, U.: The coupling of long-term trace metal trends to internal trace metal fluxes at the oxic-anoxic interface in the Gotland Basin (57° 19,20′ N; 20° 03,00′ E) Baltic Sea, J. Mar. Sys, 56, 207–225, 2005.

Pohl, C. and Hennings, U.: Trace metals in Baltic seawater, in: State and Evolution of the Baltic Sea, 1952–2005, Feistel, R., Nausch, G., and Wasmund, N. (eds.), Wiley, Hoboken, 367–393, 2008.

Pohl, C., Löffler, A., and Hennings, U.: A sediment trap flux-study for trace metals under seasonal aspects in the stratified Baltic Sea (Gotland Basin; 57° 19,20′ N; 20°03,00′ E), Mar. Chem., 84, 143–160, 2004.

Poulton, S. W. and Canfield, D. E.: Development of a sequential extraction procedure for iron: implications for iron partitioning in continentally derived particulates, Chem. Geol., 214, 209–221, 2005.

Radic, A., Lacan, F., and Murray, J. W.: Iron isotopes in the seawater of the equatorial Pacific Ocean: new constraints for the oceanic iron cycle, Earth Plan. Sci. Lett., 306, 1–10, 2011.

Rose, A. L. and Waite, T. D.: Kinetic model for Fe(II) oxidation in seawater in the absence and presence of natural organic matter, Environ. Sci. Techn., 36, 433–444, 2002.

Rouxel, O. J., Bekker, A., and Edwards, K. J.: Iron isotope constraints on the Archean and Paleoproterozoic ocean redox state, Science, 307, 1088–1091, 2005.

Rouxel, O., Sholkovitz, E., Charette, M., and Edwards, J. K.: Iron isotope fractionation in subterranean estuaries, Geochim. Cosmochim. Acta, 72, 3413–3430, 2008.

Santana-Casiano, J. M., Gonzales-Davila, M., and Millero, F. J.: The role of Fe(II) species in the oxidation of Fe(II) in natural waters in the presence of O_2^- and H_2O_2, Mar. Chem., 99, 70–82, 2006.

Schoenberg, R. and von Blanckenburg, F.: An assessment of the accuracy of stable Fe isotope ratio measurements on samples with organic and inorganic matrices by high-resolution multicollector ICP-M S, Int. J. Mass Spec., 242, 257–272, 2005.

Schoenberg, R., Zink, S., Staubwasser, M., and von Blanckenburg, F.: The stable Cr isotope inventory of solid earth reservoirs determined by double spike MC-ICP-M S, Chem. Geol., 249, 294–306, 2008.

Severmann, S., Johnson, C. M., Beard, B. L., and McManus, J.: The effect of early diagenesis on the Fe isotope compositions of porewaters and authigenic minerals in continental margin sediments, Geochim. Cosmochim. Acta, 70, 2006–2022, 2006.

Severmann, S., Lyons, T. W., Anbar, A., McManus, J., and Gordon, G.: Modern iron isotope perspective on the benthic iron shuttle and the redox evolution of ancient oceans, Geology, 36, 487–490, 2008.

Severmann, S., McManus, J., Berelson, W. M., and Hammond, D. E.: The continental shelf benthic iron flux and its isotope composition, Geochim. Cosmochim. Acta, 74, 3984–4004, 2010.

Skulan, J. L., Beard, B. L., and Johnson, C. M.: Kinetic and equilibrium Fe isotope fractionation between aqueous Fe(III) and hematite, Geochim. Cosmochim. Acta, 66, 2995–3015, 2006.

Staubwasser, M., von Blanckenburg, F., and Schoenberg, R.: Iron isotopes in the early marine diagenetic iron cycle, Geology, 34, 629–632, 2006.

Strady, E., Pohl, C., Yakushev, E. V., Krüger, S., and Hennings, U.: PUMP-CTD-System for trace metal sampling with a high vertical resolution, a test in the Gotland Basin, Baltic Sea, Chemosphere, 70, 1309–1319, 2008.

Teutsch, N., Schmid, M., Müller, B., Halliday, A. N., Bürgmann, H., and Wehrli, B.: Large iron isotope fractionation at the oxic-anoxic boundary in Lake Nyos, Earth Plan. Sci. Lett., 285, 52–60, 2009.

Welch, S. A., Beard, B. L., Johnson, C. M., and Bratemann, P. S.: Kinetic and equilibrium Fe isotope fractionation between aqueous Fe(II) and Fe(III), Geochim. Cosmochim. Acta, 67, 4231–4250, 2003.

Wijsman, J. W. M., Middelburg, J. J., and Heip, C. H. R.: Reactive iron in Black Sea sediments: implications for iron cycling, Mar. Geol., 172, 167–180, 2001.

Wu, J.: Determination of picomolar iron in seawater by double $Mg(OH)_2$ precipitation isotope dilution high-resolution ICPMS, Mar. Chem., 103, 370–381, 2007.

Yemenicioglu, S., Erdogan, S., and Tugrul, S.: Distribution of dissolved forms of iron and manganese in the Black Sea, Deep-sea Res., 53, 1842–1855, 2006.

Table 1. δ^{56}Fe of Fe_{dis} and Fe_{SPM} in the Eastern Gotland Basin.

Depth (m)	Notes	Sal	O_2 (ml l^{-1})	Fe dissolved dissolved Fe (nM)	Fe dissolved dissolved δ^{56}Fe	Fe dissolved dissolved ± 2se	Fe SPM Fe (nM)	Fe SPM δ^{56}Fe	Fe SPM ± 2se
5		6.82	6.87	13.0			6.1		
20	average	6.83	6.87	15.3	0.06	0.11	6.6	−0.12	0.08
	replicate				0.19	0.11			
	replicate				−0.06	0.11			
50		7.47	7.49	23.8	−0.17	0.12	9.6	−0.23	0.08
75		8.53	4.26	18.0			26.5		
80					0.27	0.09		−0.37	0.09
100		10.79	0.12	36.4	(0.55)**	(0.09)**	36.9	−0.61	0.09
115		11.43	0.11		0.28	0,.11		−0.24	0.09
120		11.73	0.09	18.6			29.0		
130		11.96	0.05	34.6	−0.19	0.08	59.3	−0.41	0.09
140		12.18	0.03	41.9	−0.30	0.09	48.1	−0.33	0.09
150	average	12.29	0.07	66.3	−0.40	0.09	24.4	−0.31	0.09
	replicate				−0.43	0.08			
	replicate				−0.38	0.09			
160	average	12.37	−0.75*	101.1	−0.40	0.09	9.6	−0.20	0.09
	replicate				−0.36	0.10			
	replicate				−0.45	0.09			
170	average				−0.39	0.09		−0.11	0.09
	replicate				−0.46	0.08			
	replicate				−0.33	0.09			
180		12.50	−0.75*	448.0			17.1		
190	average				−0.44	0.08		−0.09	0.08
	replicate				−0.37	0.08			
	replicate				−0.52	0.08			
200		12.60	−0.87*	445.4			29.5		

*H_2S as negative oxygen (= ml l^{-1} $H_2S \cdot 2$, Grasshoff et al., 1983),
**Discarded (see text).

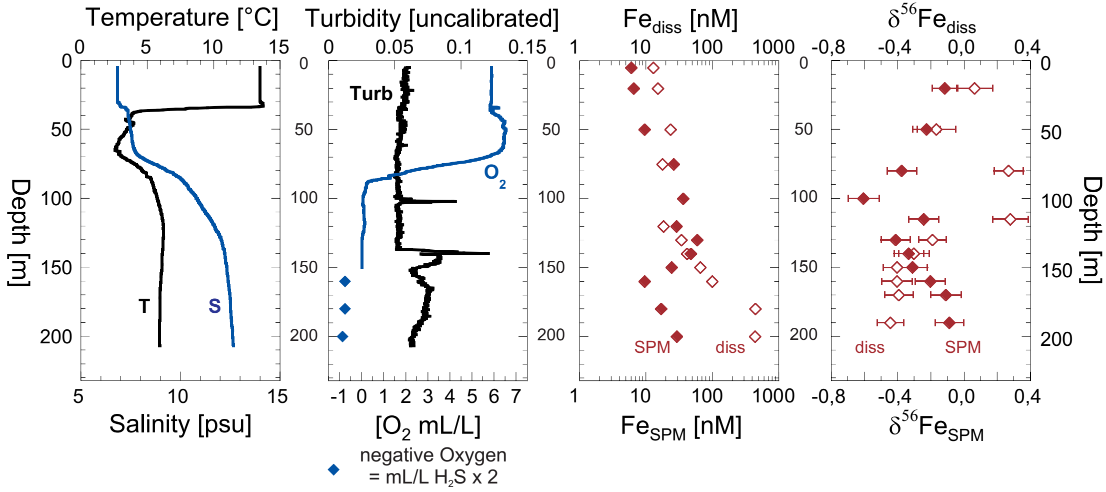

Fig. 1. Water column profile data for the Eastern Gotland Deep, Central Baltic Sea, during October 2005: **(a)** temperature and salinity; **(b)** turbidity sensor data and dissolved oxygen concentration; H_2S is presented as negative oxygen (Grasshof et al., 1983); **(c)** concentration of soluble and suspended particulate Fe; **(d)** Fe isotope ratios (δ^{56}Fe) of soluble and suspended particulate Fe.

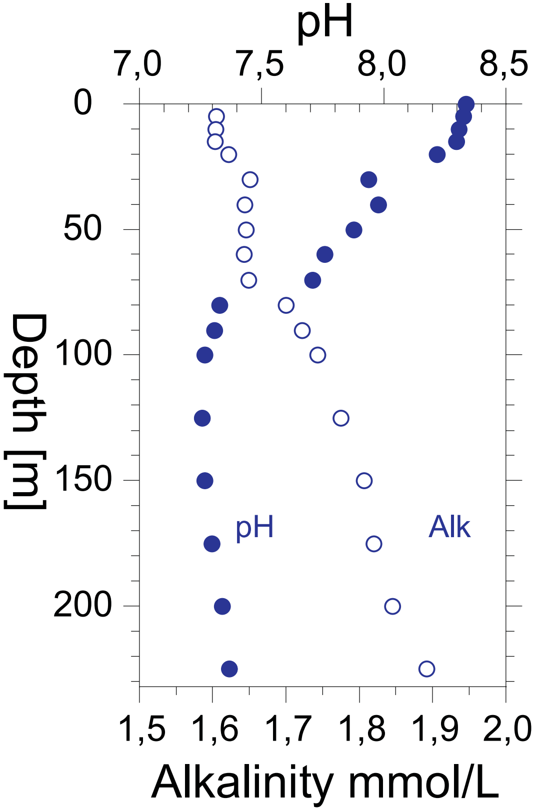

Fig. 2. Profiles of pH and alkalinity in fall 2005 for the Eastern Gotland Basin. Data are from the Swedish Meteorological and Hydrological Institute's monitoring program (Karlson et al., 2009), station BY-15 (which is identical to station 271 of this study).